OPEN ACCESS

Original research

Structural and functional correlates of the response to deep brain stimulation at ventral capsule/ventral striatum region for treatment-resistant depression

Yijie Lai ,[1] Lulin Dai,[1] Tao Wang,[1] Yingying Zhang,[2] Yijie Zhao,[3,4] Fengting Wang,[1] Qimin Liu ,[5] Shikun Zhan,[1] Dianyou Li,[1] Haiyan Jin,[6] Yiru Fang,[7] Valerie Voon,[3,4,8] Bomin Sun [1]

► Additional supplemental material is published online only. To view, please visit the journal online (http://dx.doi.org/10.1136/jnnp-2022-329702).

For numbered affiliations see end of article.

Correspondence to
Professor Bomin Sun, Department of Neurosurgery, Ruijin Hospital, Shanghai 200025, China; sbm11224@rjh.com.cn
Valerie Voon; vv247@cam.ac.uk

Received 2 June 2022
Accepted 11 December 2022
Published Online First 30 December 2022

ABSTRACT

Background Though deep brain stimulation (DBS) shows increasing potential in treatment-resistant depression (TRD), the underlying neural mechanisms remain unclear. Here, we investigated functional and structural connectivities related to and predictive of clinical effectiveness of DBS at ventral capsule/ventral striatum region for TRD.

Methods Stimulation effects of 71 stimulation settings in 10 TRD patients were assessed. The electric fields were estimated and combined with normative functional and structural connectomes to identify connections as well as fibre tracts beneficial for outcome. We calculated stimulation-dependent optimal connectivity and constructed models to predict outcome. Leave-one-out cross-validation was used to validate the prediction value.

Results Successful prediction of antidepressant effectiveness in out-of-sample patients was achieved by the optimal connectivity profiles constructed with both the functional connectivity ($R=0.49$ at $p<10^{-4}$; deviated by 14.4±10.9% from actual, $p<0.001$) and structural connectivity ($R=0.51$ at $p<10^{-5}$; deviated by 15.2±11.5% from actual, $p<10^{-5}$). Frontothalamic pathways and cortical projections were delineated for optimal clinical outcome. Similarity estimates between optimal connectivity profile from one modality (functional/structural) and individual brain connectivity in the other modality (structural/functional) significantly cross-predicted the outcome of DBS. The optimal structural and functional connectivity mainly converged at the ventral and dorsal lateral prefrontal cortex and orbitofrontal cortex.

Conclusions Connectivity profiles and fibre tracts following frontothalamic streamlines appear to predict outcome of DBS for TRD. The findings shed light on the neural pathways in depression and may be used to guide both presurgical planning and postsurgical programming after further validation.

WHAT IS ALREADY KNOWN ON THIS TOPIC

⇒ Deep brain stimulation (DBS) in ventral capsule/ventral striatum (VC/VS) showed potential in improving treatment-resistant depression (TRD), while the underlying neural mechanisms remain unclear and where or how to optimise targeting and stimulation remains poorly understood.

WHAT THIS STUDY ADDS

⇒ This is the first study providing insights into beneficial neural connections of VC/VS-DBS for TRD in both functional and structural views. It delineated a frontothalamic pathway and connectivity profile responsive for clinical outcome in VC/VS-DBS for TRD. In addition, it also provided both functional and structural evidence to support that VC/VS-DBS and subcallosal cingulate DBS may share common responsive brain network.

HOW THIS STUDY MIGHT AFFECT RESEARCH, PRACTICE OR POLICY

⇒ This study contributed to guiding in refining stimulation parameters in VC/VS-DBS for TRD in a brain network manner and understanding the neural mechanism for both invasive and non-invasive stimulations, like TMS targeting the relevant cortical areas within the responsive network.

INTRODUCTION

Deep brain stimulation (DBS) targeting the ventral capsule/ventral striatum (VC/VS) showed potential in treating treatment-resistant depression (TRD).[1] However, the published trials of VC/VS-DBS for TRD have provided inconsistent findings.[2 3] Given the divergence of the clinical effect and large number of tracts coursing through the VC/VS region, a plausible explanation might be related to suboptimal targeting of effective fibre tracts and related brain network.[3–5] This hypothesis is partly supported by the emerging understanding that DBS may exert its therapeutic effect via interactions with distributed brain networks, which painted a broad picture where the shared neural network may be responsible for the clinical effectiveness.[6 7]

Compared with ablative procedures, the stimulated brain regions of DBS, as well as the consequent therapeutic effect, can be optimised by adjusting the stimulation settings.[4 8 9] Advanced neuroimaging has identified potential trajectories around the subcallosal cingulate gyrus which may relate to optimal response.[10] Although adjusting DBS settings may lead to better clinical outcomes for TRD, where or how to optimise stimulation in VC/VS-DBS remains

Check for updates

To cite: Lai Y, Dai L, Wang T, *et al*. *J Neurol Neurosurg Psychiatry* 2023;**94**:379–388.

poorly understood.[11] Recent electrophysiological studies[12–15] and imaging analysis[10 16 17] have provided valuable insights into the electrophysiological biomarkers and white matter pathways associated with clinical effectiveness. Thus far, the published VC/VS-DBS human data for TRD focused on clinical efficacy, whereas the neural pathways correlated with the effectiveness remain elusive.

Recent advances in neuroimaging facilitate the use of the human connectome in determining connectivity profiles and brain networks that are related to symptoms and predictive of outcomes in obsessive-compulsive disorder (OCD) and Parkinson's disease (PD).[18 19] The current study tests the potential utility of both structural and functional connectome in identifying brain connectivity profiles and fibre tracts that are related to the clinical outcome of VC/VS-DBS in TRD. Here, we hypothesise that the effectiveness of VC/VS-DBS in TRD is associated with a connectivity pattern that has discernable neural fibre tracts traversing the stimulated region. We further hypothesise that the stimulation-dependent connectivity profiles would predict individual outcomes in out-of-sample data.

MATERIALS AND METHODS

Participants

Patients with TRD who were considered for neurosurgery at Ruijin Hospital from April 2021 to July 2021 were recruited for the imaging study. Subjects signed the consent form prior to the initiation of any other study-related procedures. Details for inclusion and exclusion criteria for TRD patients eligible for neurosurgery are described in online supplemental methods.

Surgical procedure

Electrodes were implanted bilaterally in the VC/VS region using stereotactic frame-based, magnetic resonance technique using SR1202-S 8-contact leads (8 contacts of 1.5 mm with a spacing of 0.5 mm; SceneRay, Suzhou, China). The most distal contact was located approximately at: X-axis=4–8 mm lateral to the midline, Y-axis=1–3 mm anterior to the anterior border of the anterior commissure and Z-axis=5–8 mm inferior to the anterior commissure. Electrodes were connected to a subcutaneous stimulator (SR1103; SceneRay) in an infraclavicular pocket. The effectiveness and safety of each electrode contact were assessed by an initial programming session 1 week after the surgery. Chronic stimulation was then delivered and adjusted every 2 weeks based on the improvement of depression symptoms (details of programming in online supplemental methods).[5]

Clinical assessment and image acquisition

Clinical outcome was measured by 17-item Hamilton depression rating scale (HAMD-17), Montgomery-Asberg Depression Rating Scale (MADRS)[20] and 14-item Hamilton anxiety rating scale (HAMA).[21] The assessments were conducted presurgically and postsurgically at each programming session. The criteria for response and remission were ≥50% reduction of HAMD-17 score from baseline and HAMD score ≤7, respectively.[9]

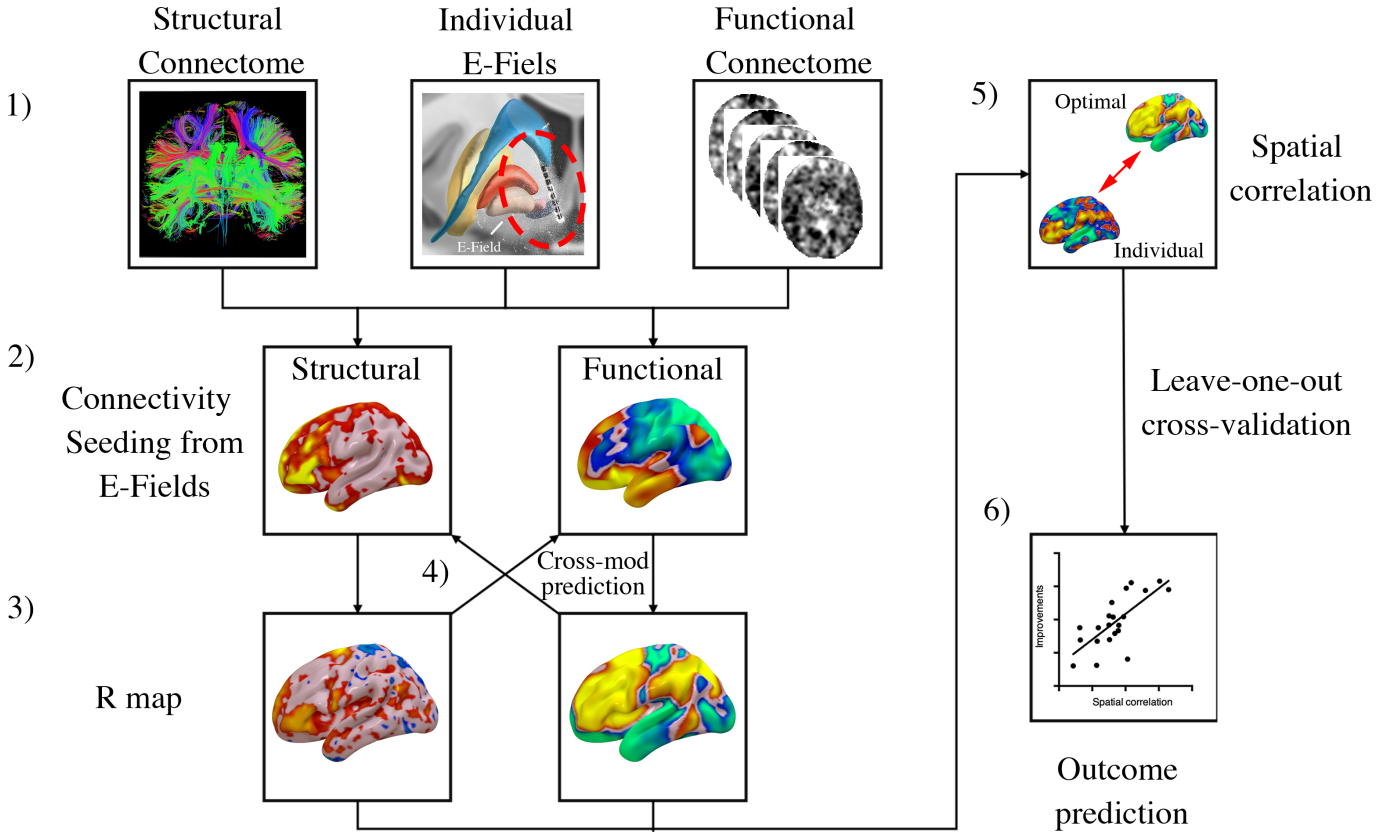

Figure 1 General workflow for creating optimal connectivity profile and predicting outcome. Processing steps include (1) acquiring preoperative/postoperative imaging, localising DBS electrodes in standard space and calculating the E-field based on stimulation parameters; (2) calculating functional/structural connectivity between the E-field and each voxel of the brain; then by incorporating outcome data, (3) R-maps were created to serve as the optimal relative distribution of connectivity; (5) calculating spatial correlation describing the similarity between individual's connectivity and the R-map; (6) finally, the prediction value was tested using leave-one-out cross-validation. DBS, deep brain stimulation.

Table 1 Characteristics of included patients

Items	Values
Number of patients	10
Number of stimulation settings	71
Sex	1 F/ 9 M
Age (years)	33.9±9.0
Disease duration (years)	16.1±8.7
Last follow-up time (months)	7.4±3.3
Follow-up time for DBS settings (weeks)	7.6±7.8
MoCA	26.6±2.0
HAMA-14	21.2±8.1
HAMD-17	20.5±2.9
MADRS	29.2±6.7
Voltage (V)	L 4.1±0.7/R 4.1±0.6
Frequency (Hz)	L 156.6±43.9/R 156.6±43.9
Pulse width (μs)	L 173.5±15.2/R 173.5±15.2

F, female; L, left; M, male; MDD, major depressive disorder; MoCA, Montreal Cognitive Assessment; R, right.

Presurgical imaging was performed on a 3T MRI system (Ingenia, Philips Medical Systems, the Netherlands). Details of sequence parameters are found in online supplemental methods.

Connectivity estimation and fibre tracking

Localisation of DBS electrodes and calculation of corresponding electric fields (E-fields) were implemented using Lead-DBS software (details in online supplemental methods).[22] Subsequently, voxel-wised functional and structural connectivity seeding from bilateral E-fields were estimated using normative data sets retrieved from the Brain Genomics Superstruct Project (GSP, fMRI from 1570 subjects in total and 1000 subjects were chosen and processed)[23] and Human Connectome Project at Massachusetts General Hospital (32 subjects, multishell diffusion-weighted imaging data),[19] respectively. Seeding from voxels within the E-field, voxel-wised connectivity profiles were calculated using Lead-DBS.[22] Values in E-fields served as weights to generate the connectivity profile. For each patient, fibres passing through a non-zero voxel of the E-field were selected from the normative connectome and projected onto a voxelised volume in standard space (2 mm resolution) while keeping count of the fibres traversing each voxel. Each fibre received the weight of the maximal E-field magnitude of its passage and fibre densities were weighted by these values. Details of connectivity estimation are found in online supplemental methods.

Table 2 Brain regions with significant differences in e-field-seeded functional connectivity between remission and non-remission subjects

Significant clusters (peak)	Peak MNI coordinate of significant clusters			Cluster size (voxels)	Peak T value
	X	Y	Z		
Functional connectivity					
Remission>non-remission					
Midbrain	-8	−18	−12	131	4.586
Left pallidum	−14	2	0	44	4.1232
Remission<non-remission					
Right caudate	8	8	-2	752	−5.5274
Right medial orbital superior frontal gyrus	12	46	-2	361	4.7428
Structural connectivity					
Remission>non-remission					
Right middle frontal gyrus	34	54	4	11 049	7.3223
Remission<non-remission					
Right parahippocampal gryrus	20	−20	−10	13 066	−4.6558
Right superior temporal gyrus	66	016	8	104	3.8576

MNI, Montreal Neurological Institute.

Isolation of fibre tracts discriminative for improvements

In the following analysis, we sought to identify tracts that could discriminate patients with different extent of HAMD-17 change using Lead-DBS.[22 24] For each fibre tract in the normative connectome, its accumulative E-field vector magnitude while delivering by each patient's electrode was calculated.[24] This value was then Spearman rank correlated with each patient's clinical improvement in depressive symptoms. These R-values were used to colour code fibre tracts that were positively and negatively predictive of HAMD-17 improvement. A high absolute R-value indicates the relatively strong ability in discriminating between good and poor responding E-fields or predictive for outcomes. This analysis made it possible to assign aggregated fibre R-scores to each (out-of-sample) E-field in subsequent leave-one-out cross-validation prediction analyses (details are in online supplemental methods).

Generation of connectivity profiles associated with improvements in depression

A data-driven approach which has previously been introduced in the context of PD and OCD to identify networks correlating with the clinical outcome across the sample was applied.[18 19] Based on our hypothesis, models of optimal connectivity were estimated using the method previously described by Horn *et al* (figure 1).[18 19 24] Functional/structural connectivity was first Spearman rank-correlated with postoperative per cent improvements in the HAMD-17 and also the MADRS scales under each stimulation setting, the Spearman's correlation coefficients in each voxel of this map then constitute the *R-maps*. These R-maps denote optimal relative distributions of the connectivity and the more similar a patient's connectivity profile is to this optimal map, the better the improvement would be expected.[25] Functional/structural connectivity was then assembled in a general linear model to predict the patient's improvement.

Agreement mask across functional and structural imaging modalities

To calculate the set of regions predictive for clinical outcomes regardless of imaging modality, the conception of previous 'agreement map' was adopted with modification.[26] Considering the fact that functional connectivity includes both correlation and anticorrelation, a weighted average map for functional connectivity was first calculated by weighting the corresponding whole-brain functional connectivity profile with clinical response (adjusted by subtracting the lowest improvement to avoid negative weights).[19] Then the R-maps of the two modalities (functional and structural) were superimposed and masked with functional weighted average map to generate the following agreement masks (details of mask description are found in online supplemental methods): (1) 'good correlation': weighted average $map_{func}>0 \cap R\text{-}map_{func}>0 \cap R\text{-}map_{struc}>0$, that is, voxels showed functional correlation with E-field and positively correlated with outcome in both functional and structural connectivity profile; (2) 'good anticorrelation': weighted average $map_{func}<0$

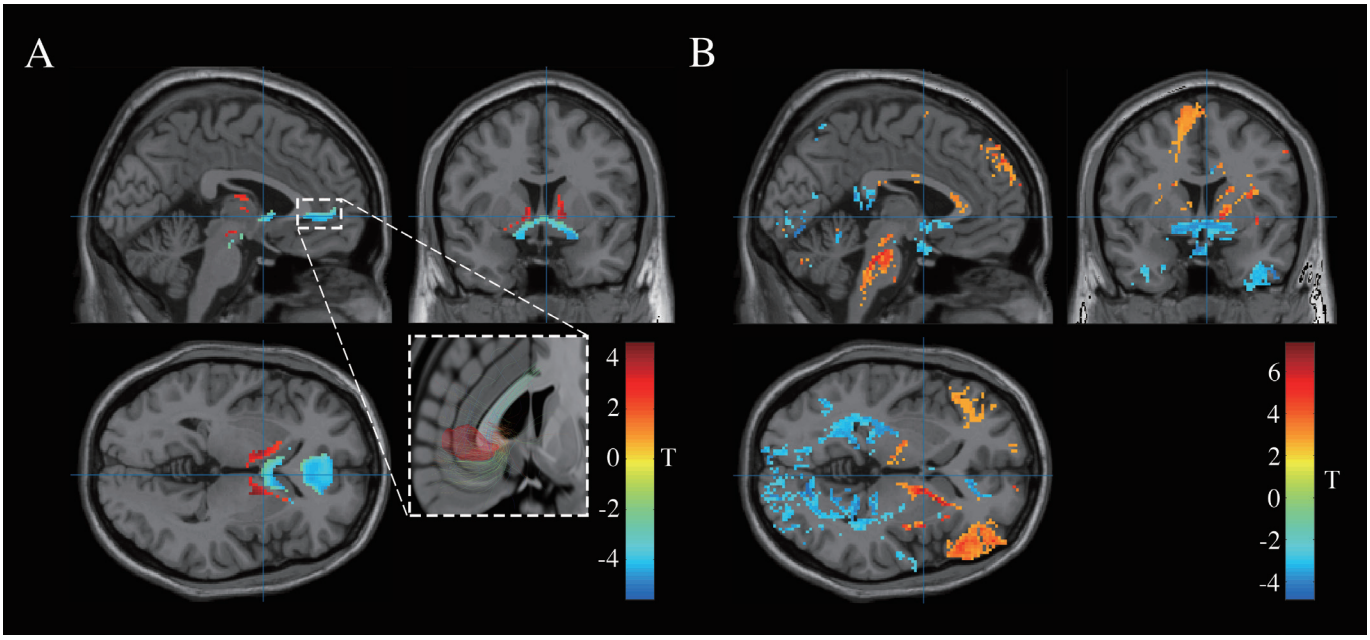

Figure 2 Connectivity differences between remission and non-remission groups. (A) Brain maps of t-statistics representing strength of positive (warm colour) or negative (cold colour) difference in functional connectivity (cluster of>100 voxels, P_{FDR}<0.05). Images within white dashes showed the investigation of normative tractography based on the corresponding functionally differed cluster (semi-opaque mass indicated the corresponding cortical areas with decrease functional connectivity). (B) Brain maps of t-statistics representing strength of positive (warm colour) or negative (cold colour) difference in structural connectivity (cluster of>100 voxels, P_{FDR}<0.05). Slices were at x=2, y=4, z=0.

$\cap$ R-map_{func}<0 $\cap$ R-map_{struc}>0; (3) 'bad correlation': weighted average map_{func}>0 $\cap$ R-map_{func}<0 $\cap$ R-map_{struc}<0, voxels showed functional correlation with E-field but negatively correlated with outcome in both structural and functional connectivity profile; (4) 'bad anticorrelation': weighted average map_{func}<0 $\cap$ R-map_{func}>0 $\cap$ R-map_{struc}<0. The agreement masks were combined to mask the functional or structural R-map for outcome prediction. Automated anatomical labelling atlas 3 (AAL-3) was used for brain parcellation (anatomical regions and abbreviation in online supplemental methods).[27] In addition, functionally defined orbitofrontal and prefrontal regions implicated in TRD including orbitofrontal cortex (OFC), dorsolateral PFC (dlPFC), ventrolateral PFC (vlPFC) and ventromedial (vmPFC) were manually defined and used in previous publications from our group.[28] We hypothesised that regions retained in the agreement mask could be more specific for clinical outcomes in both modalities.

Statistical analysis

Data were first tested for distribution using the Kolmogorov-Smirnov test, and then parametric (paired two-sample t test or Pearson's correlation coefficient) or non-parametric (paired Wilcoxon rank-sum test or Spearman's correlation coefficient) statistic was used to assess potential differences or correlation. A multivariate linear regression analysis was used to evaluate the association between clinical/demographic characteristics and the response. Independent variables included gender, age at surgery, patient number (1–10), duration of TRD at surgery, follow-up time since surgery and since each programming session, presurgical HAMD-17 and Montreal Cognitive Assessment scores. The seed-based connectivity was subjected to voxel-based analysis using statistical parametric mapping. Statistical significance was defined as p<0.05 by two-tailed tests. The false discovery rate (FDR) was used to address the multiple comparison issues. All analyses were done in MATLAB (The Mathworks, Natick, Massachusetts, USA).

RESULTS

Overall patient characteristics

A total of 71 stimulation settings on 20 leads in 10 patients (9 men; age=33.9±9.0 years) who received VC/VS-DBS for depression were included in this study (table 1). Ten subjects with TRD had a mean reduction of 55.8±20.3% in HAMD-17 score, 46.6±26.0% in MADRS score and 45.2±21.1% in HAMA-14 score at 7.4±3.3 months after surgery. After a mean observation of 7.6±7.8 weeks from programming, these 71 settings in 10 patients displayed a mean improvement of 56.5±20.2% in HAMD-17 score, 47.1±26.4% in MADRS score and 39.3±31.5% in HAMA-14 score. Fourty-one (57.7%) of these 71 settings reached response (≥50% reduction in HAMD-17) and 27 (38.0%) were at remission (≤7 on HAMD-17). In the multivariate analysis, the included variables displayed insignificant contributions to the improvement in HAMD-17 (all ps>0.05) except for presurgical HAMD-17 scores (p=0.020). The results of electrode reconstruction demonstrated relative accuracy of implantation across all subjects and the major portion of the E-field overlapped with the ventral half of the internal capsule (online supplemental figure 1).

Functional and structural connectivity differences in response groups

Based on the AAL-3 parcellation, the remission group showed increased functional connectivity (towards the positive end) peaking at two clusters (table 2 and figure 2A): (1) midbrain (131 voxels), which includes right ventral anterior thalamus and left and right red nucleus and (2) left pallidum (PAL; 44 voxels). The remission group showed decreased functional connectivity (towards the negative end) peaking at: (1) right caudate (CAU; 752 voxels), this cluster also overlapped with various subcortical structures, such as bilateral putamen, bilateral nucleus accumbens and bilateral PAL; (2) right medial orbital superior

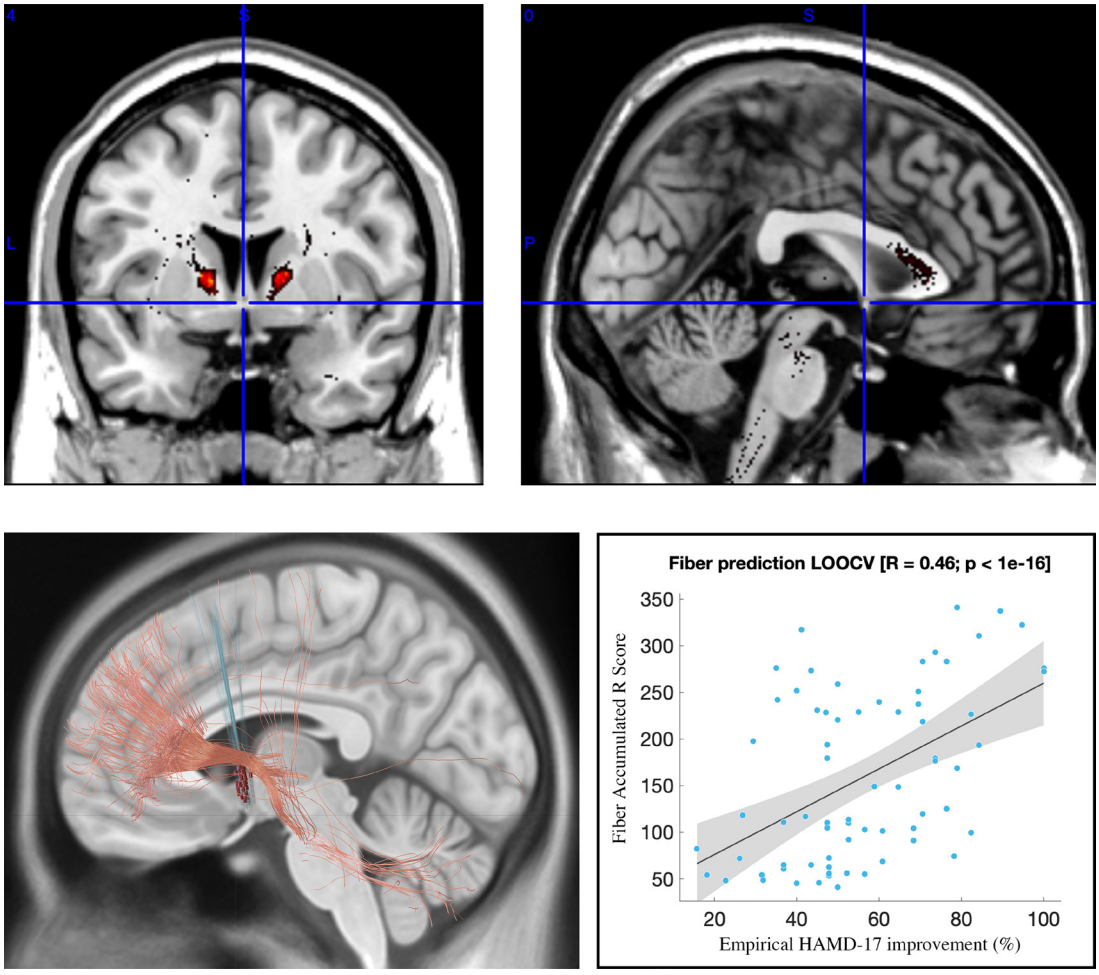

Figure 3 Fibre tracts discriminative of HAMD-17 improvement when modulated. Red tracts are positively correlated with clinical improvement. Upper left and right showed the relative location of the tracts at coronal and sagittal views in T1-weighted MRI MNI152 NLIN 2009b slices. Lower left, predictive fibres positively associated with clinical improvement shown in red. Only positive fibres are shown here for reasons of clarity. The top 50% predictive fibres are displayed. Lower right, correlations between the degree of stimulating positively predictive tracts (sum of aggregated fibre R-scores under each E-field) and clinical improvements. Grey shaded areas represent 95% CI. HAMD, Hamilton depression rating scale; LOOCV, leave-one-out cross-validation; MNI, Montreal Neurological Institute;.

frontal gyrus (PFCventmed; 361 voxels), this cluster also overlapped with various cortical areas, including bilateral medial superior frontal gyrus (SFGmedial) and bilateral supracallosal and pregenual anterior cingulate cortex (ACCpre and ACCsup). Interestingly, further tractography analysis based on this cluster showed aside from the frontothalamic projections, it also has bunches of fibre tracts connected to subcallosal cingulate (figure 3A).

Similarly, the remission group showed increased structural connectivity peaking at the right middle frontal gyrus (11 049 voxels), which included a large area of the bilateral frontal cortex, the left supplementary motor area (SMA), bilateral ACC and subcortical structures (table 2 and figure 2B). The remission group also showed decreased structural connectivity peaking at: (1) right parahippocampal gyrus (13 066 voxels), this cluster also overlapped with a large range of voxels mainly in bilateral temporal, occipital and lingual gyrus and (2) right superior temporal gyrus (STG; 104 voxels).

No significant group difference was found in the E-field-based seed-to-voxel functional or structural connectivity between responders and non-responders (FDR corrected ps>0.05).

Fibre tracts related to improvements after VC/VS–DBS

In the following analysis, we identified the actual tracts (instead of their cortical projection sites) of which modulation was correlated with HAMD-17 improvement. A positively correlated tract starting from the midbrain and then traversing through the ventral half of the internal capsule at the level of stimulation mainly to the medial and lateral prefrontal cortex was identified in the cohort (figure 3), it was at the vicinity of mainly the dorsal half of the contacts in current study (online supplemental figure 2). Through the leave-one-out cross-validation, the degree of lead connectivity in an out-of-sample patient to this tract significantly predicted clinical improvement (figure 3, R=0.46 at $p<10^{-16}$).

Optimal connectivity map construction and prediction of VC/VS-DBS outcomes

As described in figure 1 and the Methods section, R-map models (structural and functional R-maps) were calculated on data from the 71 available programming settings using normative structural/functional connectome to predict HAMD-17 improvement (figure 4). Similarity estimates between the maps

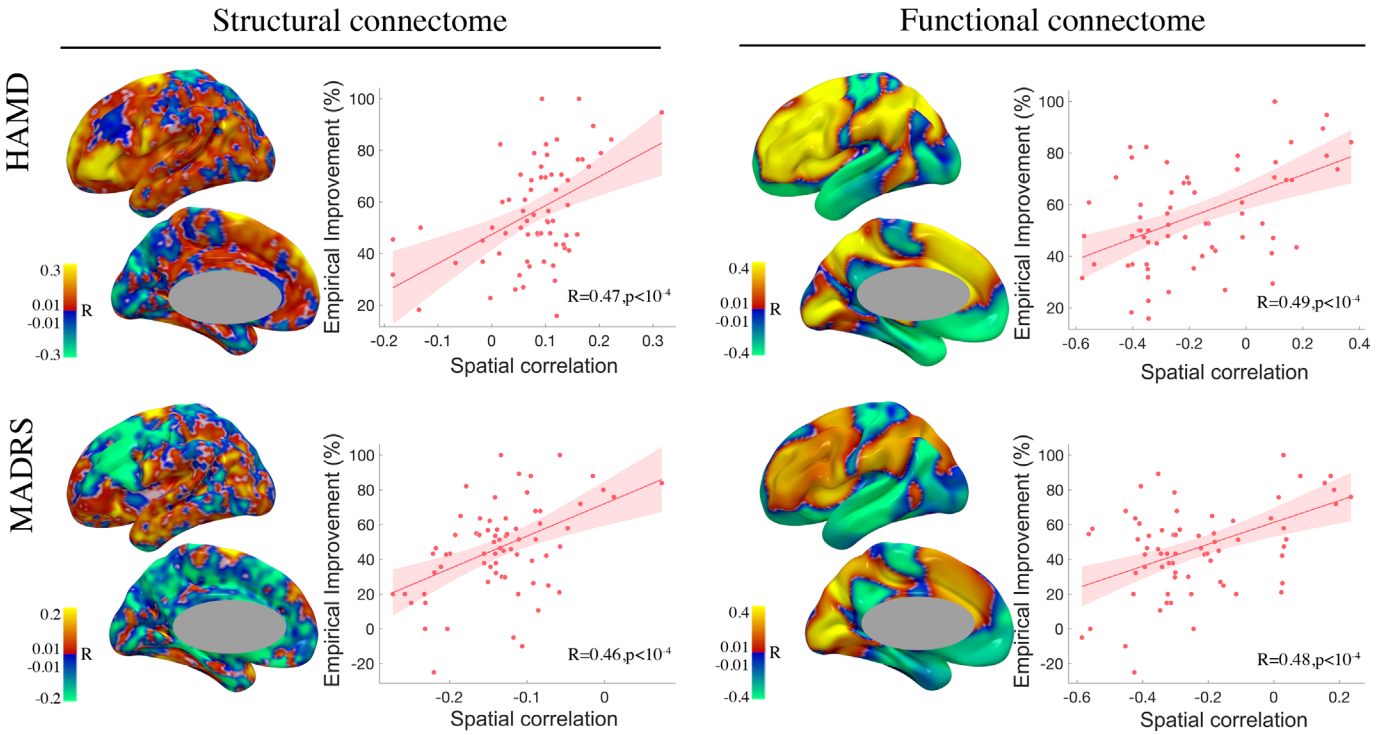

Figure 4 Leave-one-out cross-validation of prediction of HAMD-17 and MADRS score improvement using connectivity seeding from E-field. Similarity between patient-specific structural or functional connectivity profile and R-map constructed with structural or functional connectivity profile was used to predict improvement in HAMD-17 and MADRS score. Pink areas represent the 95% CI. HAMD, Hamilton depression rating scale; MADRS, Montgomery-Asberg Depression Rating Scale.

and each out-of-sample whole-brain connectivity fingerprint significantly predicted clinical improvements (figure 4 top left and right; R=0.51 at $p<10^{-5}$ and R=0.49 at $p<10^{-4}$). To test its efficiency across different measures for depression, the above two maps were, respectively, constructed based on the improvement measured with MADRS (figure 4 lower left and right). Both structural and functional R-maps showed the capacity to predict improvement in MADRS (figure 5 lower left, structural R-map, R=0.53, $p<10^{-5}$; and right, functional R-map, R=0.48, $p<10^{-4}$). By assembling the structural connectivity information into a GLM model, the predictive outcome deviated by 15.2±11.5% (R=0.51, $p<10^{-5}$) from actual improvements as measured by per cent changes in HAMD-17 scores and deviated by 14.4±10.9% (R=0.43, p<0.001) with the use of functional connectivity information.

Cross-prediction across structural and functional modalities and agreement masks

Next, we examined if it was possible to predict outcomes based on the similarity of functional R-maps and structural connectivity profiles and vice versa. Though the structural and functional R-maps showed discrepancies in figure 1, they became increasingly similar as the R-scores increased (figure 5). The amount of variance explained decreased but was still significant by the cross-prediction process compared with using R-map and its matched connectivity profile (figure 5, R=0.26 and p=0.028 for using functional R-map and structural connectivity; R=0.42 and p<0.001 for using structural R-map and functional connectivity).

Finally, we aimed at creating an agreement mask within which the connectivity profile would be maximally predictive regardless of imaging modalities. As illustrated in the section Methods and figure 6A, the functional and structural connectivity information were combined to map areas represented for correlation and anticorrelation related to superior outcome ('good correlation' and 'good anticorrelation'), and also those related to the inferior ones ('bad correlation' and 'bad anti-correlation'). Voxels in these areas were combined to create the agreement mask, which was used to mask the functional and structural R-maps for outcome prediction. The masked models were significantly predictive of outcome and showed slightly better performance in leave-one-out cross-validation compared with the unmasked profiles in both the functional (R=0.49, $p<10^{-4}$; figure 6B) and structural connectivity (R=0.49, $p<10^{-4}$; figure 6B). By averaging the portion of involved voxels of brain regions within these four mapped areas in 71 leave-one-out models, the 'good correlation' area overlapped mainly at regions of frontal gyrus, thalamus and SMA (figure 6C). In the subdivisions of prefrontal cortex, the 'good correlation' area overlapped at 21.8% of dlPFC, 17.6% of vlPFC and also 9.8% of OFC, while no voxels overlapped with vmPFC. The 'good anticorrelation' area overlapped mainly at regions of temporal cortex, occipital cortex and postcentral gyrus (online supplemental figure 3), which only overlapped with 0.6% of dlPFC and no voxels in vlPFC, vmPFC and OFC. The tractography of the cross-modality mask beneficial for outcome (areas with good correlation/anticorrelation) showed that the fibres traversing through the internal capsule resided mainly at the ventral half of the internal capsule and correlated with electrode locations as well as the predictive fibre tracts identified in figure 3 (online supplemental figure 3).

DISCUSSION

In this pilot imaging study, we first characterised connectivity patterns predictive of outcome in patients with TRD following VC/VS−DBS. Then we delineated a tractographic target that was predictive of the clinical outcome within the frontothalamic

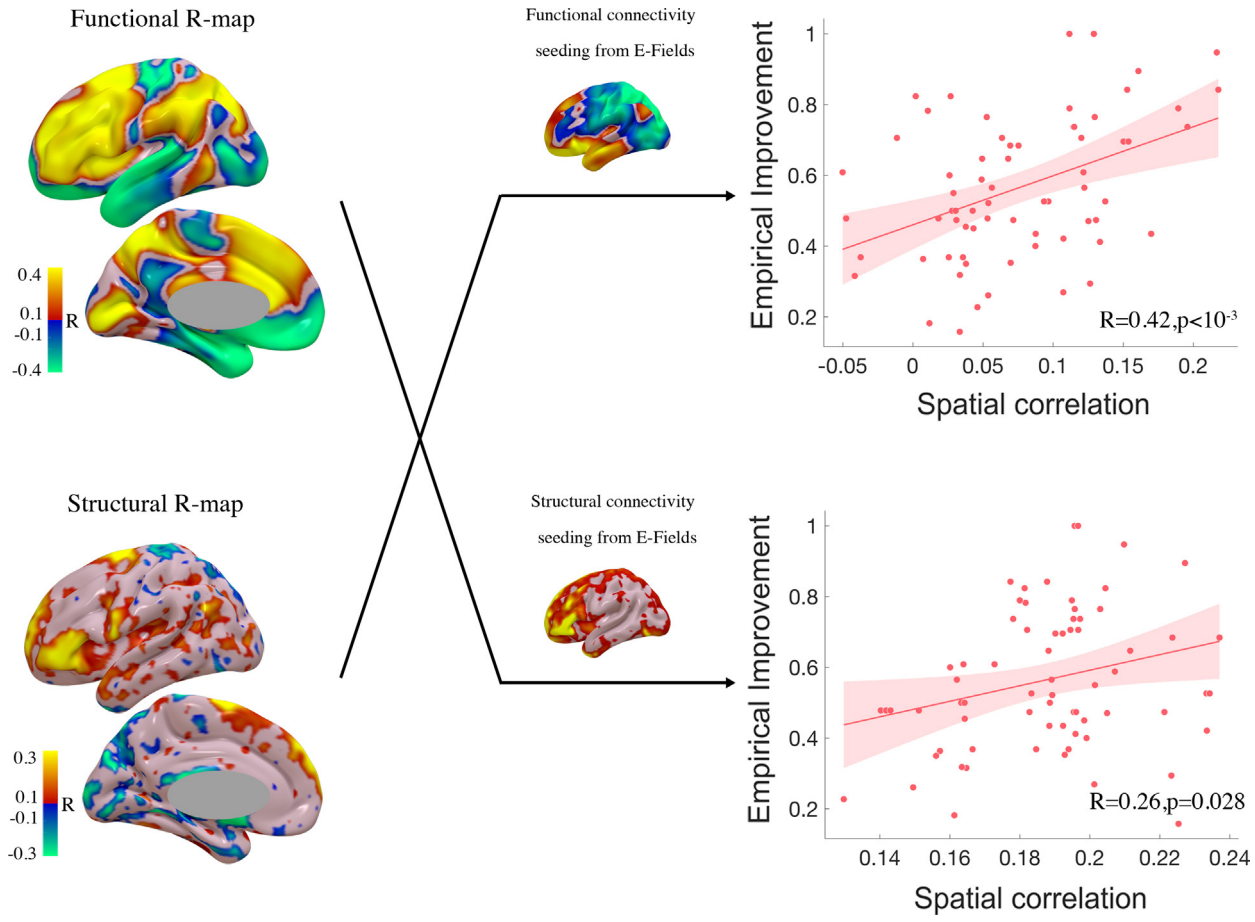

Figure 5 Cross-predicting DBS outcomes across functional and structural connectomes. R-maps for both functional connectivity (top left) and structural connectivity (bottom left) were used to crosspredict clinical improvements in HAMD-17 in the other cohort, respectively (top right shows predictions of outcomes using similarity between R-map constructed from structural connectivity and the patient-specific functional connectivity profile, bottom right shows predictions of outcomes using similarity between R-map constructed from functional connectivity and the patient-specific structural connectivity profile). Pink areas represent the 95% CI. DBS, deep brain stimulation; HAMD-17, 17-item Hamilton depression rating scale. Lower limits were thresholded at R=0.1.

radiation. Finally, we identified the brain regions where beneficial structural and functional connections may converge. We found an optimal stimulation connectivity profile for both structural and functional connectivity encompassing mainly the ventral and dorsal lateral PFC and OFC. Additionally, the relevant tractography analysis of functional differed areas between response groups revealed potential link between VC/VS-DBS and DBS targeting the subcallosal cingulate area-DBS, suggesting a shared responsive brain network may exist for both targets. These findings shed light on clinical practice for both presurgical planning and postoperative programming and provide insights into fundamental mechanisms.

Compared with the relatively founded basal-ganglia model for movement disorders, the mechanism under psychiatry diseases remains largely clouded. A better understanding of implicated neural circuits is necessary as it promotes more informed ways to deliver treatment. Converging animal and human studies have linked the pathophysiology of depression to dysfunction in reward processing, which comprises a brain network centred on the VS.[29] Hypothesis-driven open-label studies have been conducted targeting various nodes within the reward network with DBS for TRD, including VC/VS, ventral anterior limb of the internal capsule, bed nucleus of the stria terminalis, inferior thalamic peduncle and the lateral habenula.[1 30–32] Since VC/VS stimulation might have a broad effect on emotional and motivational processes, efficacy likely depends on the modulation of specific connections or axon bundles travelling through the VC/VS[2]

This study adopted the idea that specifying responsive neural connections or related axon bundles might help increase clinical response.[17] Our first step in navigating cortical projection sites revealed optimal whole-brain structural and functional connectivity that would be predictive. Moreover, via cross-prediction, optimal whole-brain structural and functional connectivity profiles of VC/VS–DBS for effective treatment of TRD showed similarity across brain regions. For both connectivity modalities, an enhanced positive connectivity profile within ventral and dorsal lateral PFC and OFC appears to be associated with optimal clinical outcomes (figure 6). This finding is in line with previous studies demonstrating that DBS could significantly increase metabolism in dlPFC after 1 week of stimulation.[33] Also, the optimal functional connectivity profile identified in the current study was largely identical to the one described by Siddiqi *et al*, which was established based on results from various targets, including VC/VS, subgenual anterior cingulate cortex, subthalamic nucleus and anterior nucleus of the thalamus, in lesional as well as stimulation surgery.[7]

In our analysis of fibre tracts that may be responsible for the outcome, a positively correlative tract that started from the midbrain and then traversed through the ventral half of the internal capsule at the level of stimulation mainly to the medial prefrontal cortex and vlPFC was identified in the cohort.[28] The

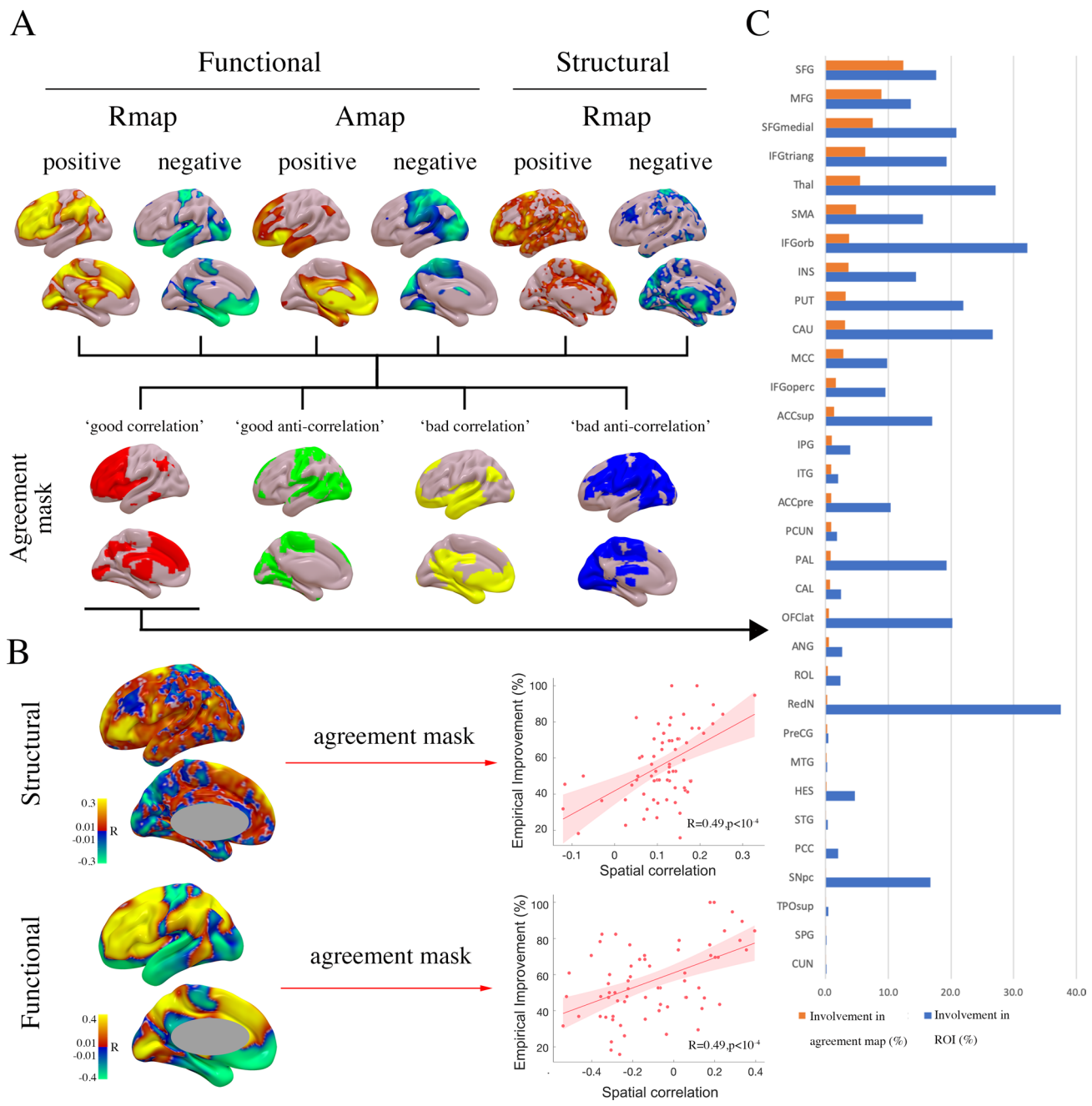

Figure 6 Agreement masks between structural and functional modalities. (A) Brief pipeline for creating agreement masks and illustration of 'good correlation', 'good anti-correlation', 'bad correlation' and 'bad anti-correlation' agreement masks; (B) leave-one-out cross-validation of prediction of HAMD-17 score improvement using connectivity profiles masked by agreement masks. Pink areas represent the 95% CI. C, percentage involvement in 'good correlation' agreement mask by ROIs in AAL-3 brain parcellation. ROIs were analysed bilaterally. HAMD-17, 17-item Hamilton depression rating scale; ROI, region of interest; SFG, superior frontal gyrus, dorsalateral; MFG, middle frontal gyrus; IFGtriang, inferior frontal gyrus, triangular part; Thal, thalamus; SMA, supplementary motor area; IFGorb, inferior frontal gyrus, pars orbitalis; INS, insula; PUT, putamen; CAU, caudate; MCC, middle cingulate & paracingulate gyri; IFGoperc, inferior frontal gyrus, opercular part; ACCsup, anterior cingulate cortex, supracallosal; IPG, inferior parietal gyrus; ITG, inferior temporal gyrus; ACCpre, anterior cingulate cortex, pregenual; PCUN, precuneus; PAL, pallidum; CAL, calcarine fissure and surrounding cortex; OFClat, lateral orbital gyru; ANG, angular gyrus; ROL, rolandic operculum; RedN, red nucleus; PreCG, precentral gyrus; MTG, middle temporal gyrus; HES, heschl's gyrus; STG, superior temporal gyrus; PCC, posterior cingulate gyrus; SNpc, substantia nigra, pars compacta; TPOsup, temporal pole: superior temporal gyrus; SPG, superior parietal gyrus; CUN, precuneus.

pathway was highly similar to that described by Li *et al* responsive for OCD.[34] This is not unexpected for depression and OCD given that psychiatric diseases are dimensional and can share transdiagnostically similar symptoms, including anxiety, relatively low mood and social withdrawal. They also overlap through partially common pharmacological treatments suggesting overlapping structural and functional disease correlates. Our findings add support to the emerging concept that OCD, major depressive disorder and other psychiatric disorders are network disorders that can be targeted through stimulation.[17]

This study also has the advantage of investigating both the functional and structural correlates of DBS effectiveness in TRD.

The structural and functional connectivity separately offers information on space and time, and consideration for both characteristics of pathophysiological networks may offer the greatest promise to optimise clinical outcomes for future DBS technologies.[35 36] Fibre tract and connectivity from normative connectomes might be expected to assist in future preoperative surgical planning and guiding postoperative programming in prospective cohorts.[37] Researchers can selectively focus on neuromodulation of these corresponding areas to achieve ideal outcome, for example, increasing the connectivity/stimulation coverage of areas with good correlation/anticorrelation and decreasing the connectivity/stimulation coverage of areas with bad ones. Further studies using controlled trials might lead to changes in clinical practice to guide postoperative programming, by generating multiple E-fields based on different sets of stimulation parameters, then picking the set of parameters that generate the E-field whose connectivity predicts the highest improvement.

Limitation

This study had several drawbacks. First, the implantation could result in microlesion effect, which might interfere with the responses.[11] To minimise the microlesion effect, only visits with follow-up for above 1 month from surgery were included. Second, though the follow-up time since surgery and since each programming session were found not correlated with the outcome, the acute, for example, immediately after programming, or long-term, for example, months' or years', antidepressant effects were not thoroughly discussed in this study.[38] Finally, our study revealed beneficial connections in an average human brain, while it did not account for individual variations of connectivity, we further caution that patient-specific functional or structural imaging data would be valuable.[36] However, individualised connectivity may also add additional noise to the analysis.[39]

CONCLUSIONS

The results of this preliminary imaging investigation indicated that specific connectivity profiles and fibre tracts could predict the clinical outcome of DBS for TRD. The functional and structural responsive regions mainly converged on the PFC. The findings shed light on the neural pathways in depression and may be used to guide both presurgical planning and postsurgical programming after further validation. In the future, more refined models should help in predicting the parameter combinations that are effective for an individual patient or a specific symptom profile.

Author affiliations
[1]Department of Neurosurgery, Ruijin Hospital, Shanghai Jiao Tong University School of Medicine, Shanghai, China
[2]Department of Neurosurgery, Clinical Neuroscience Center Comprehensive Epilepsy Unit, Ruijin Hospital, Shanghai Jiao Tong University School of Medicine, Shanghai, China
[3]Institute of Science and Technology for Brain-Inspired Intelligence, Fudan University, Shanghai, China
[4]Key Laboratory of Computational Neuroscience and Brain-Inspired Intelligence (Fudan University), Ministry of Education, Shanghai, China
[5]Department of Psychology and Human Development, Vanderbilt University, Nashville, Tennessee, USA
[6]Department of Psychiatry, Ruijin Hospital, Shanghai Jiao Tong University School of Medicine, Shanghai, China
[7]Clinical Research Center and Division of Mood Disorders, Shanghai Mental Health Center, Shanghai Jiao Tong University School of Medicine, Shanghai, China
[8]Department of Psychiatry, Cambridge University, Cambridge, UK

Correction notice This article has been corrected since it was first published. The open access licence has been updated to CC BY.

Acknowledgements We thank Dr Lifu Deng and Dr. Tianzhu Xiong for valuable advice on imaging data processing.

Contributors YL, YF, VV and BS contributed to the conception and design of the study. YL, LD, TW, FW, SZ, DL and HJ contributed to acquisition, post-processing and analysis of the data. YL, YZ, QL, VV and BS drafted the text and prepared the figures. All authors approved the final version of the manuscript.

Funding This deep brain stimulation intervention was supported by an unrestricted, investigator-initiated research grant by Scenery Inc (Drs Sun and Li), which provided the devices used. The project was sponsored by SJTU Trans-med Awards Research (2019015 to Dr. Sun), Shanghai Clinical Research Centre for Mental Health (19MC191100 to Dr. Sun) and Shanghai Municipal Science and Technology Commission (21DZ1100303 to Dr. Sun). Dr. Sun was also sponsored by the National Natural Science Foundation of China (81771482). Dr. Voon was supported by the Guangci Professorship Programme of Ruijin Hospital and a Medical Research Council Senior Clinical Fellowship (MR/P008747/1). Dr. Lai was sponsored by the National Natural Science Foundation of China (82101546) and the Shanghai Sailing Program (21YF1426700). The funding sources were not involved in the design and conduct of the study; collection, management, analysis, and interpretation of the data; preparation, review, or approval of the manuscript; and decision to submit the manuscript for publication.

Competing interests Drs Sun and Li receive occasional fees from Scenery for educational purposes. No other conflicts were reported.

Patient consent for publication Not applicable.

Ethics approval All procedures were approved by the ethics committee of Ruijin Hospital Shanghai Jiao Tong University School of Medicine (approval number: 202152). Participants gave informed consent to participate in the study before taking part.

Provenance and peer review Not commissioned; externally peer reviewed.

Data availability statement Data are available upon reasonable request.

ORCID iDs
Yijie Lai http://orcid.org/0000-0003-4443-0136
Qimin Liu http://orcid.org/0000-0003-3840-1136
Bomin Sun http://orcid.org/0000-0001-5931-2197

REFERENCES

1 Dandekar MP, Fenoy AJ, Carvalho AF, *et al*. Deep brain stimulation for treatment-resistant depression: an integrative review of preclinical and clinical findings and translational implications. *Mol Psychiatry* 2018;23:1094–112.
2 Dougherty DD, Rezai AR, Carpenter LL, *et al*. A randomized sham-controlled trial of deep brain stimulation of the ventral Capsule/Ventral striatum for chronic treatment-resistant depression. *Biol Psychiatry* 2015;78:240–8.
3 Richardson RM, Ghuman AS, Karp JF. Results of the first randomized controlled trial of deep brain stimulation in treatment-resistant depression. *Neurosurgery* 2015;77:N23–4.
4 Zhang C, Lai Y, Li J, *et al*. Subthalamic and pallidal stimulations in patients with Parkinson's disease: common and dissociable connections. *Ann Neurol* 2021;90:670–82.
5 Bergfeld IO, Mantione M, Hoogendoorn MLC, *et al*. Deep brain stimulation of the ventral anterior limb of the internal capsule for treatment-resistant depression: a randomized clinical trial. *JAMA Psychiatry* 2016;73:456–64.
6 Baldermann JC, Schüller T, Kohl S, *et al*. Connectomic deep brain stimulation for obsessive-compulsive disorder. *Biol Psychiatry* 2021;90:678–88.
7 Siddiqi SH, Schaper FLWVJ, Horn A, *et al*. Brain stimulation and brain lesions converge on common causal circuits in neuropsychiatric disease. *Nat Hum Behav* 2021;5:1707–16.
8 Bergfeld IO. Putting deep brain stimulation for depression in a wider perspective. *Lancet Psychiatry* 2020;7:2–3.

9 Ramasubbu R, Clark DL, Golding S, *et al*. Long versus short pulse width subcallosal cingulate stimulation for treatment-resistant depression: a randomised, double-blind, crossover trial. *Lancet Psychiatry* 2020;7:29–40.
10 Riva-Posse P, Choi KS, Holtzheimer PE, *et al*. A connectomic approach for subcallosal cingulate deep brain stimulation surgery: prospective targeting in treatment-resistant depression. *Mol Psychiatry* 2018;23:843–9.
11 Bhati MT, Halpern CH. Deciphering deep brain stimulation for depression. *Lancet Psychiatry* 2017;4:820–1.
12 Sheth SA, Bijanki KR, Metzger B, *et al*. Deep brain stimulation for depression informed by intracranial recordings. *Biol Psychiatry* 2022;92:246–51.
13 Scangos KW, Khambhati AN, Daly PM, *et al*. Closed-loop neuromodulation in an individual with treatment-resistant depression. *Nat Med* 2021;27:1696–700.
14 Sonkusare S, Ding Q, Zhang Y, *et al*. Power signatures of habenular neuronal signals in patients with bipolar or unipolar depressive disorders correlate with their disease severity. *Transl Psychiatry* 2022;12:72.
15 Zhang C, Zhang Y, Luo H, *et al*. Bilateral habenula deep brain stimulation for treatment-resistant depression: clinical findings and electrophysiological features. *Transl Psychiatry* 2022;12:52.
16 Riva-Posse P, Choi KS, Holtzheimer PE, *et al*. Defining critical white matter pathways mediating successful subcallosal cingulate deep brain stimulation for treatment-resistant depression. *Biol Psychiatry* 2014;76:963–9.
17 Coenen VA, Schlaepfer TE, Sajonz B, *et al*. Tractographic description of major subcortical projection pathways passing the anterior limb of the internal capsule. Corticopetal organization of networks relevant for psychiatric disorders. *Neuroimage Clin* 2020;25:102165.
18 Baldermann JC, Melzer C, Zapf A, *et al*. Connectivity profile predictive of effective deep brain stimulation in obsessive-compulsive disorder. *Biol Psychiatry* 2019;85:735–43.
19 Horn A, Reich M, Vorwerk J, *et al*. Connectivity predicts deep brain stimulation outcome in Parkinson disease. *Ann Neurol* 2017;82:67–78.
20 Montgomery SA, Asberg M. A new depression scale designed to be sensitive to change. *Br J Psychiatry* 1979;134:382–9.
21 Hamilton M. Development of a rating scale for primary depressive illness. *Br J Soc Clin Psychol* 1967;6:278–96.
22 Horn A, Li N, Dembek TA, *et al*. Lead-DBS V2: towards a comprehensive pipeline for deep brain stimulation imaging. *Neuroimage* 2019;184:293–316.
23 Cohen A, Soussand L, McManus P. *GSP1000 preprocessed connectome*. V3. Harvard Dataverse, 2020.
24 Irmen F, Horn A, Mosley P, *et al*. Left prefrontal connectivity links subthalamic stimulation with depressive symptoms. *Ann Neurol* 2020;87:962–75.
25 Horn A, Ostwald D, Reisert M, *et al*. The structural-functional connectome and the default mode network of the human brain. *Neuroimage* 2014;102 Pt 1:142–51.
26 Sobesky L, Goede L, Odekerken VJJ. Subthalamic and pallidal deep brain stimulation: are we modulating the same network? *Brain : a journal of neurology* 2021.
27 Rolls ET, Huang C-C, Lin C-P, *et al*. Automated anatomical labelling atlas 3. *Neuroimage* 2020;206:116189.
28 Morris LS, Kundu P, Dowell N, *et al*. Fronto-striatal organization: defining functional and microstructural substrates of behavioural flexibility. *Cortex* 2016;74:118–33.
29 Satterthwaite TD, Kable JW, Vandekar L, *et al*. Common and dissociable dysfunction of the reward system in bipolar and unipolar depression. *Neuropsychopharmacology* 2015;40:2258–68.
30 van der Wal JM, Bergfeld IO, Lok A, *et al*. Long-term deep brain stimulation of the ventral anterior limb of the internal capsule for treatment-resistant depression. *J Neurol Neurosurg Psychiatry* 2020;91:189–95.
31 Huys D, Kohl S, Baldermann JC, *et al*. Open-label trial of anterior limb of internal capsule-nucleus accumbens deep brain stimulation for obsessive-compulsive disorder: insights gained. *J Neurol Neurosurg Psychiatry* 2019;90:805–12.
32 Fenoy AJ, Quevedo J, Soares JC. Deep brain stimulation of the "medial forebrain bundle": a strategy to modulate the reward system and manage treatment-resistant depression. *Mol Psychiatry* 2022;27:574–92.
33 Schlaepfer TE, Cohen MX, Frick C, *et al*. Deep brain stimulation to reward circuitry alleviates anhedonia in refractory major depression. *Neuropsychopharmacology* 2008;33:368–77.
34 Li N, Baldermann JC, Kibleur A, *et al*. A unified connectomic target for deep brain stimulation in obsessive-compulsive disorder. *Nat Commun* 2020;11:3364.
35 Wu C, Ferreira F, Fox M, *et al*. Clinical applications of magnetic resonance imaging based functional and structural connectivity. *Neuroimage* 2021;244:118649.
36 Lai Y, He N, Wei H, *et al*. Value of functional connectivity in outcome prediction for pallidal stimulation in Parkinson disease. *J Neurosurg* 2022:1–11.
37 Horn A, Fox MD. Opportunities of connectomic neuromodulation. *Neuroimage* 2020;221:117180–80.
38 Ashkan K, Rogers P, Bergman H, *et al*. Insights into the mechanisms of deep brain stimulation. *Nat Rev Neurol* 2017;13:548–54.
39 James GA, Kelley ME, Craddock RC, *et al*. Exploratory structural equation modeling of resting-state fMRI: applicability of group models to individual subjects. *Neuroimage* 2009;45:778–87.

Structural and functional correlates of response to deep brain stimulation at ventral capsule/ventral striatum region for treatment-resistant depression

Supplementary Information

Supplementary Methods

Inclusion Criteria: Subjects aged 18-65 years old who were able to provide informed consent were included. Inclusion criteria included psychiatrist-confirmed International Classification of Diseases, 10th revision (ICD-10) diagnostic criteria for major depressive disorder; ≥ 17 on the 17-item Hamilton depression rating scale (HAMD) and medical record documentation that each patient's current major depressive episode persisted for ≥ 2 years or ≥ 4 recurrences with a current episode lasting ≥ 1 year.[1] Treatment resistance was defined as a lack of clinically substantive response to at least 3 or more adequate trials of antidepressant therapy, including 8 or more weeks of 2 or more different classes of antidepressants (eg, selective serotonin reuptake inhibitor, tricyclic antidepressant, tricyclic antidepressant with lithium augmentation, monoamine oxidase inhibitor); at least 1 session of electroconvulsive therapy (ECT), for which the series of ECT was terminated either due to adverse effects or insufficient response (including at least 6 sessions of bilateral ECT), or unable to receive ECT; poor improvement after at least 6 weeks of psychotherapy treatment for the current or a previous depressive episode. Patients who fulfilled the above criteria and remained stable with the current antidepressive regimen for the last month were eligible.

Exclusion criteria were schizophrenia or psychosis unrelated to MDD, severe personality disorder or

neurological disorders (e.g., Parkinson's disease, dementia, epilepsy, tic disorder), organic brain disorders (e.g., tumor, cerebral vascular diseases), history of brain surgery and contraindications for anesthesia or stereotactic surgery. Subjects with contraindications for surgery such as major medical comorbidities or the use of anticlotting medications that could not be discontinued were also excluded.

Post-operative programming: The effectiveness and safety of each electrode contact was assessed by an initial programming session 1 week after the surgery. Trained psychiatrists and neurosurgeons tested each contact individually through careful parameter titration with monopolar stimulation. The amplitude was gradually increased at a 0.5V stepwisely from 2V with fixed frequency (130Hz) and pulse width (90μs). With the stimulator as anode (+), each electrode, beginning with the most distal one, was stimulated as monopolar cathode (−) with an increasing amplitude to a maximum of 6 V for 30-60 s, as long as no acute adverse effects were elicited. If little clinical improvement was achieved following standardized optimization, we tested voltages greater than 6.0 V and adjustments in pulse width and frequency. Induction of beneficial effects or adverse effects were documented. If beneficial effects were noted, the respective electrode was chosen with minimal adverse effect. Chronic stimulation settings were chosen based on the above testing and adjusted every two weeks based on the improvement of depression symptoms.[2]

Image Acquisition: Pre-surgical imaging was performed on a 3T MRI system (Ingenia, Philips Medical Systems, the Netherlands). The MRI protocol consisted of the following sequences: axial three-dimensional T1-weighted Turbo-Field-Echo sequence (TR/TE 6.99/3.42 ms, voxel size 0.75x0.75x1.5mm3, FOV 240x240 mm2), and axial T2-weighted fast spin-echo (T2 TSE; TR/TE 4000/106 ms, voxel size 0.6x0.6x1.5mm3, FOV 240x240 mm2). Postoperative CT scans were also acquired. High-resolution images were acquired on a

LightSpeed16 (GE Medical System, Milwaukee, WI, USA) slice CT with a spatial resolution of 0.49x0.49x0.67mm3. Images were acquired in axial (i.e., sequential/incremental) order at 140 kV and automated mA setting. The noise index was 7.0. A large scan FOV with a 50 cm diameter was used.

DBS Lead Localization: DBS electrodes were localized using Lead-DBS using the PaCER algorithm.[3] In brief, postoperative CT images were first linearly coregistered to preoperative MRI and normalized into ICBM 2009b NLIN asymmetric space using the SyN approach implemented in Advanced Normalization Tools. DBS electrodes were then localized using Lead-DBS and warped into the Montreal Neurological Institute (MNI) space using the PaCER algorithm after visual review and refinement of the coregistrations and normalizations.[4] Anatomical segmentations of local subcortical structures at the DBS site as defined by the CIT-168 atlas.[5]

Electric Fields Estimation: Electric fields (E-fields) were calculated applying a finite element method (FEM)-based model in each patient.[3] Conductivities of 0.33 and 0.14S/m were assigned to gray and white matter, respectively. Based on the volume conductor model, the potential distribution was simulated using the integration of the FieldTrip-SimBio pipeline. The surface of the volume mesh served as the anode. Subsequently, the gradient of the potential distribution was calculated by derivation of the FEM solution.

The anatomical regions defined in AAL-3 used in this study and their abbreviations.

No.	Anatomical description	Abbreviation	No.	Anatomical description	Abbreviation
1	Precentral gyrus	PreCG	30	Fusiform gyrus	FFG
2	Superior frontal gyrus, dorsolateral	SFG	31	Postcentral gyrus	PoCG
3	Middle frontal gyrus	MFG	32	Superior parietal gyrus	SPG

4	Inferior frontal gyrus, opercular part	IFGoperc	33	Inferior parietal gyrus, excluding supramarginal and angular gyri	IPG
5	Inferior frontal gyrus, triangular part	IFGtriang	34	SupraMarginal gyrus	SMG
6	IFG pars orbitalis	IFGorb	35	Angular gyrus	ANG
7	Rolandic operculum	ROL	36	Precuneus	PCUN
8	Supplementary motor area	SMA	37	Paracentral lobule	PCL
9	Olfactory cortex	OLF	38	Caudate nucleus	CAU
10	Superior frontal gyrus, medial	SFGmedial	39	Lenticular nucleus, Putamen	PUT
11	Superior frontal gyrus, medial orbital	PFCventmed	40	Lenticular nucleus, Pallidum	PAL
12	Gyrus rectus	REC	41	Thalamus	THA
13	Medial orbital gyrus	OFCmed	42	Heschl's gyrus	HES
14	Anterior orbital gyrus	OFCant	43	Superior temporal gyrus	STG
15	Posterior orbital gyrus	OFCpost	44	Temporal pole: superior temporal gyrus	TPOsup
16	Lateral orbital gyrus	OFClat	45	Middle temporal gyrus	MTG
17	Insula	INS	46	Temporal pole: middle temporal gyrus	TPOmid
18	Anterior cingulate & paracingulate gyri	ACC	47	Inferior temporal gyrus	ITG
19	Middle cingulate & paracingulate gyri	MCC	48	Anterior cingulate cortex, subgenual	ACCsub
20	Posterior cingulate gyrus	PCC	49	Anterior cingulate cortex, pregenual	ACCpre
21	Hippocampus	HIP	50	Anterior cingulate cortex, supracallosal	ACCsup
22	Parahippocampal gyrus	PHG	51	Nucleus accumbens	Nacc
23	Amygdala	AMYG	52	Ventral tegmental area	VTA
24	Calcarine fissure and surrounding cortex	CAL	53	Substantia nigra, pars compacta	SNpc

25	Cuneus	CUN	54	Substantia nigra, pars reticulata	SNpr
26	Lingual gyrus	LING	55	Locus coeruleus	Red nucleus
27	Superior occipital gyrus	SOG	56	Red nucleus	Locus coeruleus
28	Middle occipital gyrus	MOG	57	Raphe nucleus, dorsal	RapheD
29	Inferior occipital gyrus	IOG	58	Raphe nucleus, median	RapheM

Functional Connectivity Estimation: Voxel-wised functional connectivity seeding from bilateral E-fields were estimated using a normative resting state functional connectivity dataset retrieved from the Brain Genomics Superstruct Project (GSP), which included 1570 subjects in total (ages 18-36), and 1000 subjects (1:1 M/F), were chosen and processed using publicly available tools to generate a normative functional connectivity dataset.[6] The original GSP data was acquired on matched Siemens 3T MAGNETOM Tim Trio MRI systems (Erlangen, Germany) using the vendor-supplied 12-channel phased-array head coil. Preprocessing included global signal regression and spatial smoothing at 6mm full width at half maximum as described.[6] Seeding from voxels within the E-field model, a voxel-wised functional connectivity profile was calculated. Values in E-fields served as weights to generate the connectivity profile using the Lead-DBS tool.[3]

Structural Connectivity Estimation and Fiber Tracking: The structural connectivity estimation and fiber tracking were implemented using Lead-DBS.[3] Briefly, voxel-wised structural connectivity profiles seeding from bilateral E-fields were estimated using a normative group connectome computed based on multishell diffusion-weighted imaging data from 32 subjects of the Human Connectome Project at Massachusetts General Hospital.[7] Whole brain tractography fiber sets were calculated using a generalized q-sampling imaging algorithm. In each subject, 200,000 fibers were sampled and then transformed into MNI space.[7] For each patient, fibers passing through a non-zero voxel of the E-field were selected from this normative connectome

and projected onto a voxelized volume in standard space (2mm resolution) while keeping count of the fibers traversing each voxel. Each fiber received the weight of the maximal E-field magnitude of its passage and fiber densities were weighted by these values.

Leave-one-out cross-validation: The value of the above connectivity profiles as well as the identified fibertracts in outcome prediction was tested by employing leave-one-out cross-validation to predict out-of-sample outcome data.[7] Firstly, connectivity data seeding from E-field from the #2-71 settings were used to create the combined optimal map, and this map was used to estimate the outcome in setting #1; then connectivity data from the #1, 3-71 settings were used to estimate the outcome in patient #2, and so on. The spatial correlation between the individual patient map and the optimal map, which was expressed as a Spearman's rank correlation coefficient, describes the similarity between a patient's brain connectivity profile and the optimal connectivity profile.[7]

Creation of agreement mask across functional and structural imaging modalities: The R-maps of the two modalities (functional and structural) were superimposed and masked with functional weighted average map to generate the following agreement masks:

1) 'good correlation': areas that were positive in three maps (weighted average $map_{func}>0 \cap$ R-$map_{func}>0 \cap$ R-$map_{struc}>0$; voxels showed functional correlation with E-field and positively correlated with outcome in both functional and structural connectivity);

2) 'good anti-correlation': areas that were positive in structural R-map, but negative in functional weighted average map and R-map (weighted average $map_{func}<0 \cap$ R-$map_{func}<0 \cap$ R-$map_{struc}>0$; voxels showed

functional anti-correlation with E-field but positively correlated with outcome in structural connectivity and negatively correlated with outcome in functional connectivity);

3) 'bad correlation': areas that were positive in functional weighted average map, but negative in functional and structural R-map (weighted average $map_{func}>0 \cap$ R-$map_{func}<0 \cap$ R-$map_{struc}<0$; voxels showed functional correlation with E-field but negatively correlated with outcome in both structural and functional connectivity);

4) 'bad anti-correlation': areas that were positive in functional R-map, but negative in functional weighted average map and structural R-map (weighted average $map_{func}<0 \cap$ R-$map_{func}>0 \cap$ R-$map_{struc}<0$; voxels showed functional anti-correlation with E-field but positively correlated with outcome in functional connectivity and negatively correlated with outcome in structural connectivity).

Compared with previous agreement map,[8] the above 4 subtypes of agreement mask were constructed without assigning connectivity strength and only informed the area but not connectivity strength, because though the presence of a functional connection may depend on the presence of a direct or indirect structural connection, the strength of a functional connection does not need to be directly related to the strength of those structural connections.[9] The agreement masks were combined to mask the functional or structural R-map for outcome prediction.

Automated anatomical labelling atlas 3 (AAL-3) was used for brain parcellation.[10] In addition, functionally defined orbitofrontal and prefrontal regions implicated in TRD including orbitofrontal cortex (OFC), dorsolateral PFC (dlPFC), ventrolateral PFC (vlPFC), and ventromedial (vmPFC) were manually defined and used in previous publications from our group (supplemental materials in Morris et al on manual definitions).[11] We hypothesized that regions retained in the agreement mask could be more specific for clinical outcomes in both modalities.

Supplementary Results

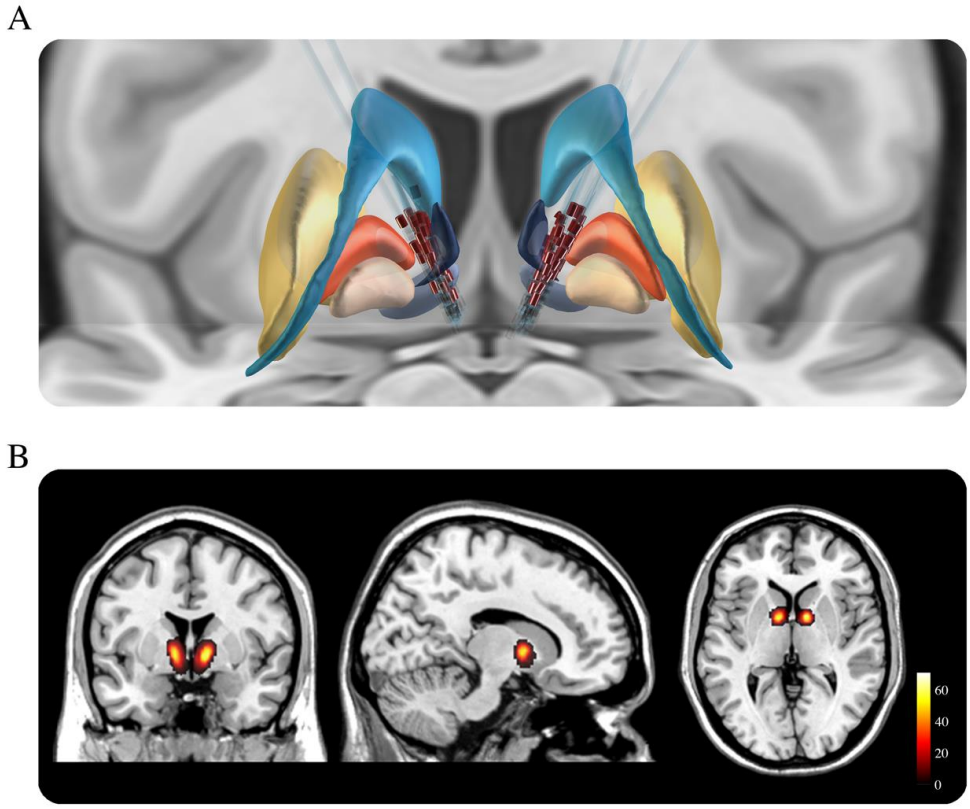

Supplementary figure 1. Location of electrodes the E-fields. A, the current corhort targeting VC/VS, subcortical structures defined by CIT-168 Atlas, with coronal and axial planes of the T1-weighted MNI152 NLIN 2009b template as background. Electrodes were made semi-transparent and active contacts are marked in red, light blue pseudocolor indicates the location of the caudate, yellow for the putamen, orange for the globus pallidus externus, light brown for the globus pallidus internus, dark blue for extensive amygdala, purple for nucleus accumbens. B, location of e-fields in coronal, sagittal and axial T1-weighted MRI (MNI152 NLIN 2009b) slices, the hot map denoted the number of binarized E-fields (thresholded at 0.2V/mm for visualization) overlapped in each voxel.

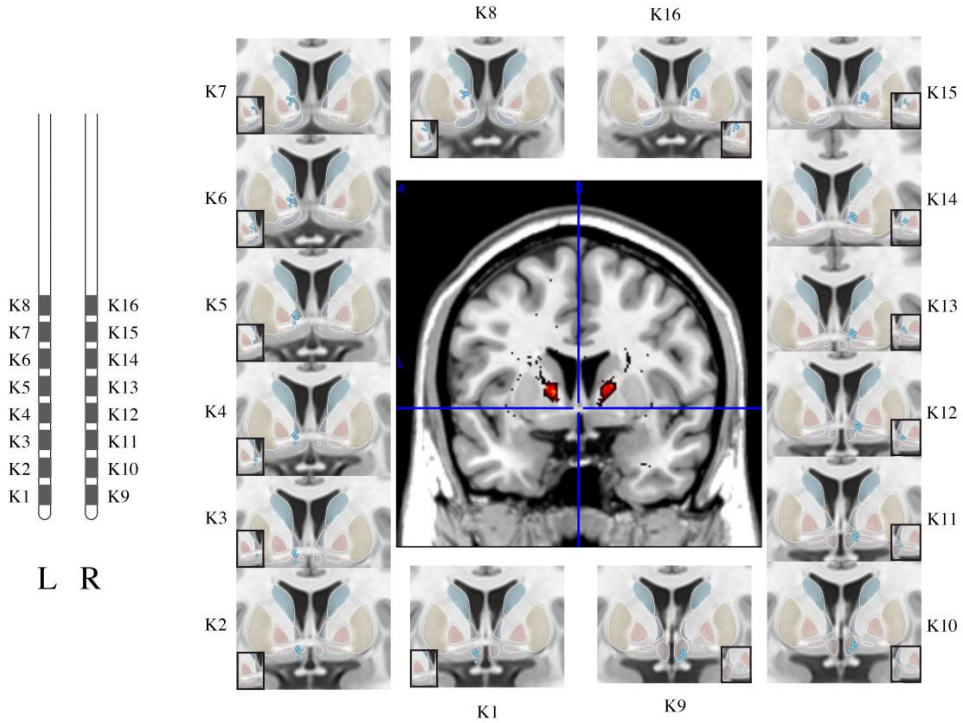

Supplementary figure 2. Contact visualization and fibertracts discriminative of HAMD-17 improvement when modulated. Red tracts in the middle image are positively correlated with clinical improvement. Contacts were shown in blue circles. Active contacts were show in black boxes at the corner of each contact image.

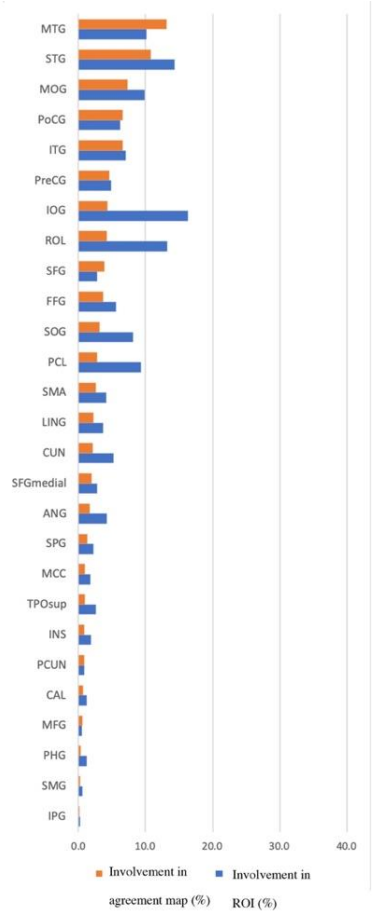

Supplementary figure 3. Percentage involvement in 'good anti-correlation' agreement mask by ROI in AAL-3 brain parcellation. ROIs were analyzed bilaterally.

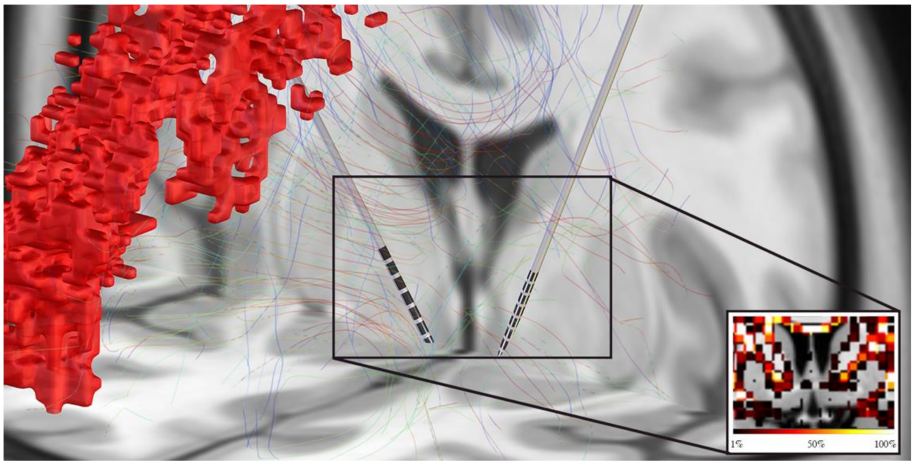

Supplementary figure 4. The whole-brain tractography of the cross-modality map beneficial for outcome in Lead-DBS software. A sample of electrode was displayed. The percent of fibers connected to the voxels relative to the max was denoted by heatmap in the black box.

Reference

1. Hamilton M. A rating scale for depression. *Journal of neurology, neurosurgery, and psychiatry* 1960;23(1):56-62. doi: 10.1136/jnnp.23.1.56.
2. Bergfeld IO, Mantione M, Hoogendoorn ML, et al. Deep Brain Stimulation of the Ventral Anterior Limb of the Internal Capsule for Treatment-Resistant Depression: A Randomized Clinical Trial. *JAMA psychiatry* 2016;73(5):456-64. doi: 10.1001/jamapsychiatry.2016.0152.
3. Horn A, Li N, Dembek TA, et al. Lead-DBS v2: Towards a comprehensive pipeline for deep brain stimulation imaging. *NeuroImage* 2019;184:293-316. doi: 10.1016/j.neuroimage.2018.08.068.
4. Husch A, M VP, Gemmar P, et al. PaCER - A fully automated method for electrode trajectory and contact reconstruction in deep brain stimulation. *NeuroImage Clinical* 2018;17:80-89. doi: 10.1016/j.nicl.2017.10.004.
5. Pauli WM, Nili AN, Tyszka JM. A high-resolution probabilistic in vivo atlas of human subcortical brain nuclei. *Scientific data* 2018;5:180063. doi: 10.1038/sdata.2018.63.
6. Cohen A, Soussand L, McManus P, et al. GSP1000 Preprocessed Connectome. V3 ed: Harvard Dataverse, 2020.
7. Horn A, Reich M, Vorwerk J, et al. Connectivity Predicts deep brain stimulation outcome in Parkinson disease. *Annals of neurology* 2017;82(1):67-78. doi: 10.1002/ana.24974.
8. Sobesky L, Goede L, Odekerken VJJ, et al. Subthalamic and pallidal deep brain stimulation: are we modulating the same network? *Brain : a journal of neurology* 2021 doi: 10.1093/brain/awab258.
9. Straathof M, Sinke MR, Dijkhuizen RM, et al. A systematic review on the quantitative relationship between structural and functional network connectivity strength in mammalian brains. *Journal of Cerebral Blood Flow & Metabolism* 2019;39(2):189-209. doi: 10.1177/0271678x18809547.
10. Rolls ET, Huang CC, Lin CP, et al. Automated anatomical labelling atlas 3. *NeuroImage* 2020;206:116189. doi: 10.1016/j.neuroimage.2019.116189.
11. Morris LS, Kundu P, Dowell N, et al. Fronto-striatal organization: Defining functional and microstructural substrates of behavioural flexibility. *Cortex* 2016;74:118-33. doi: 10.1016/j.cortex.2015.11.004.